International Symposium
On Turbulence and Shear Flow
Phenomena (TSFP-9)
June 30 - July 3, 2015 *Melbourne, Australia*

INTERACTION OF THE AIR WITH LIQUID IN PRESSURE-SWIRL SPRAYS

Jan Jedelský, Milan Malý and Miroslav Jícha
Faculty of Mechanical Engineering
Brno University of Technology
Technická 2896/2, Brno 61669, Czech Republic
jedelsky@fme.vutbr.cz

Noé Pinto del Corral
Faculty of Sciences
Universidad Autónoma de Madrid
C/Francisco Tomás y Valiente 7, 28049 Madrid, Spain
noe.pinto.delcorral@gmail.com

ABSTRACT

The flow field in a spray produced by a pressure-swirl (PS) atomizer was studied using Phase-Doppler Anemometry (PDA). A Stokes number (Stk) analysis of the sprayed droplets showed that droplets < 5 µm followed the airflow so were used to provide estimates of the local air velocity. The Stk increases with drop size; even 20–40 µm sized droplets (Stk ~ 1) are partially affected by the air flow while the largest ones (80–160 µm, Stk > 10) move ballistically. The liquid and gas flow fields were compared in terms of the mean and rms velocities. The airflow, inside the hollow-cone spray, was found to be highly anisotropic and spatially varying within three distinct regions. Spatially resolved TKE and MKE of the air and spectra of the droplet velocity fluctuations are detailed in the paper.

INTRODUCTION

PS atomizers convert the pressure energy of the pumped liquid into kinetic energy to create a high-speed conical film of liquid which discharges into the surrounding gas. The film breaks up initially due to stretching and then to aerodynamic forces. This strong liquid–gas interaction plays a substantial role in the whole of the atomization process; high-momentum liquid fragments induce an entrained air motion, which consequently controls the flow of smaller liquid fragments and results in dispersion and reposition of small droplets downstream, where collisions (Santolaya et al. 2013), droplet clustering and spray unsteadiness (Domann & Hardalupas, 2002; Luong & Sojka, 1999) occur. It affects important characteristics of fuel nozzles, such as the spray dispersion angle, drop-size and velocity distributions (Durdina et al. 2014), while the intense gas–liquid mixing promotes the fuel evaporation and decreases the demand for ignition energy (Lefebvre & Ballal, 2010).

The turbulent characteristics of the liquid-induced entrained airflow (spatial structure, isotropy and homogeneity, frequency spectra) and the size range of air affected droplets could be determined by an analysis of the size-resolved droplet and gas flow fields and used to elucidate the role of the entrained air in the spray development downstream. Amongst a number of studies on PS sprays only few deal with the phase-resolved velocity fields so a detailed measurement of the velocity of both the phases is required. The airflow is often traced using artificial seeding particles (Santolaya et al., 2013), but sprays contain droplets with a wide size range, and the smallest ones could serve as natural tracers. This concept, however, requires a detailed analysis to prove and optimise it.

In this work the air–liquid interaction is addressed to allow estimates of the spatially resolved flow fields of air and liquid within the spray based on PDA measurements of droplet size and three-component droplet velocity. The main focus is on the turbulent airflow characteristics and the effect of the air on the droplet fate.

EXPERIMENTAL

A small PS atomizer originally developed for an aircraft engine, as shown in Figure 1 and studied by Durdina et al. (Durdina et al., 2014), was investigated on an atmospheric spray bench.

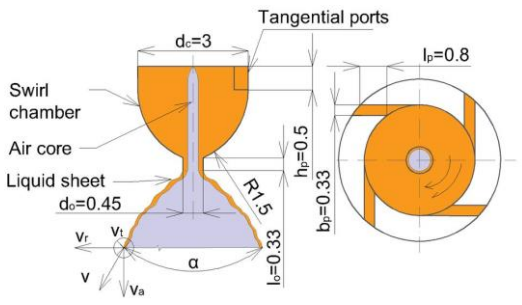

Figure 1. Atomizer geometry.

The Jet A-1 fuel with a density $\rho_l = 795$ kg/m^3, viscosity $\mu_l = 0.0016$ kg/(m·s) and surface tension $\sigma = 0.029$ kg/s^2 was sprayed at room temperature into the quiescent air. The characteristics of the sprayed liquid, i.e. the time-resolved size and velocity of the individual droplets, were probed using a two-component PDA (Jedelsky at al. 2015). The PDA measurements were performed in four radial sections of the spray at axial distances from the nozzle exit of $X = 12.5$, 25, 37.5 and 50 mm. All three velocity components (axial, radial and tangential) were measured. The nozzle was operated at inlet gauge pressures of 0.5, 1 and 1.5 MPa.

RESULTS AND DISCUSSION

The internal swirl chamber flow strongly affects the spray and, as the nozzle is too small for visualization, only simple calculations have been performed to estimate the flow character. Descriptions of the spray process are based on photographic observation in the near nozzle area and on PDA data in the developed spray.

Liquid Discharge

The liquid, fed under pressure by a pump, swirls inside the nozzle and discharges from the exit orifice with a high velocity into, initially low turbulent, quiescent air. The liquid forms a thin conical film (Figure 1, 2). The internal flow ranged Reynolds number by Walzel $\mathrm{Re}_w = \sqrt{2\rho_l \Delta p}\, d_o/\mu_l = 7930\text{–}13735$ which exceeds the critical value for turbulent transition $\mathrm{Re}_{Wc} = 5000$ (Walzel, 1993).

Strong liquid-gas interaction results from the high velocity shear between the liquid sheet and the surrounding air and, with the aid of internally induced turbulent perturbations, produce sheet deformations. Surface tension forces act on the perturbed sheet to generate perforations which are followed by ordering of the liquid fragments into horizontally oriented filaments that later break up into large droplets. This primary breakup process results in the formation of a hollow-cone spray.

The disintegration of the large drops into smaller ones, secondary breakup, takes place further downstream of the nozzle orifice and is driven by the action of aerodynamic forces (Lefebvre, 1989) and collisions between droplets. Smaller droplets decelerate in a short distance and are entrained with the air flow. The size-resolved variation in droplet velocity is documented in Figure 3. Three size regions can be identified: small droplets with $d_p < 20$ µm with a low velocity, medium size droplets in the range from 20 µm < d_p < 50 µm that show a positive size–velocity correlation and the largest droplets with a high and size independent velocity.

The air-droplet interaction leads to a size-resolved droplet radial redistribution: small droplets are transported with air into the spray centre while larger droplets move on a ballistic trajectory. The mean droplet size at each position is represented by the Sauter mean diameter, D_{32}. This parameter is frequently used in mass and heat transfer spray studies: $D_{32} = \sum_{i=1}^{n} D_i^3 \Big/ \sum_{i=1}^{n} D_i^2$. Figure 4 shows very low mean size $D_{32} < 15$ µm in $R = 0$ mm, increasing to 40 µm at $X = 12.5$ mm and even greater sizes at greater X distances downstream. An increase in drop size with axial spray development suggests liquid evaporation of the smaller droplets, collision driven coalescence, or primary break up of liquid fragments is still taking place to generate larger droplets.

Stokes Number

The interaction of particles with a surrounding media in liquid-gas two-phase flow can be explained by means of the Stokes number:

$$Stk = \rho_l C_c \bar{d}_p^{\,2} \Delta\bar{v} \big/ 18 \mu_g L\,, \qquad (1)$$

where μ_g is the air dynamic viscosity, ρ_l is the particle

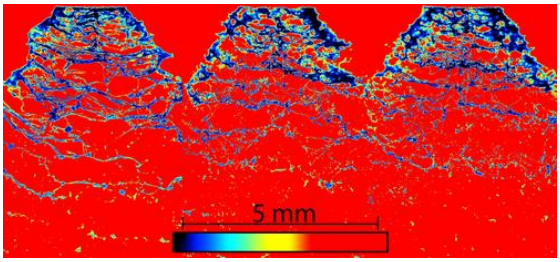

Figure 2. Breakup process of the discharged liquid sheet, $\Delta p = 0.5$, 1, 1.5 MPa. (left to right), the colour coding is used to identify the liquid structures and filamets.

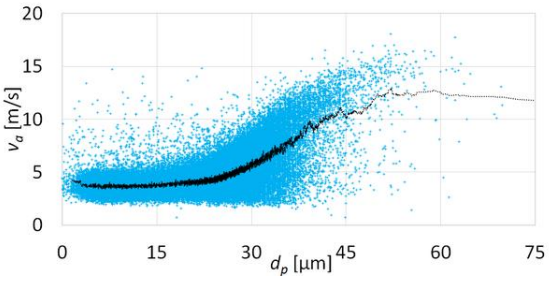

Figure 3. Drop size–vel. correlation with flowing average (black line); $X = 37.5$ mm, $R = 15$ mm, $\Delta p = 1$ MPa.

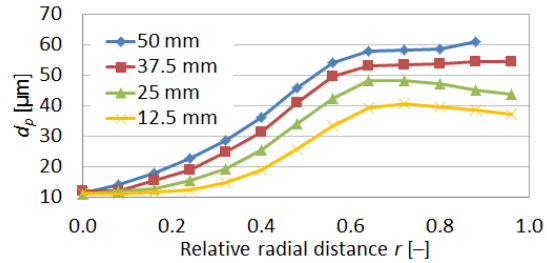

Figure 4. Radial profiles of droplet size, D_{32}; $\Delta p = 1$ MPa.

density and $\Delta\bar{v} = \left|\overrightarrow{\bar{v}_p} - \overrightarrow{\bar{v}_g}\right| = \left|\left(v_{px} - \bar{v}_{gx}\right)^2 + \ldots\right|$ is the difference, in absolute terms, between the local mean air velocity vector[1] and the mean velocity vector of the droplets. The value for $\Delta\bar{v}$ was taken as the average value of the velocity difference between the breakup point and the measurement point. The characteristic length, L, represents the distance from the breakup position to the inspected point $L = \sqrt{X^2 + R^2} - \sqrt{X_b^2 + R_b^2}$. The Cunningham correction factor $C_c \approx 1$ for the particles in our case. The particles were sorted into several size bins with an average diameter $\bar{d}_p = \left(\sum_{i=1}^{n} d_{pi}^2 \Big/ n\right)^{1/2}$[2].

The Stk increases significantly with droplet size, while the effect of radial position is minor (Figure 5, only one-half of the full radial profile is shown here and thereafter for the sake of conciseness as the spray can be considered to be axisymmetric). Particles with the size range $2.5 \le d_p < 5$ µm flow with a very low Stk ~ 0.02. Generally particles with Stk << 1 follow the airflow faithfully[3], Therefore, the velocity of particles with $d_p < 5$ µm was used to provide an estimate of the local airflow velocity. This size range, with $\bar{d}_p = 4\,\mu\text{m}$ typically, corresponds well with the size of seeding particles used for airflow studies by other authors[4].

A low Stk, however, is not the only requirement the small sprayed particles must obey to be suitable as the natural airflow tracers. Their sufficient number and frequency are required for statistical robustness and the possibility to obtain spectral characteristics respectively. The former requirement is fulfilled using a long-enough duration for the measurement and the second one is conditioned with a high data rate and drop size distribution with a great portion of small particles. These conditions are accomplished only in some spray positions. Small particles are often generated as satellite droplets and can be entrained in the wake of larger ones. In such a case, their velocity would be biased against the gas velocity. The trend in the velocity of the small droplets ($d_p < 5$ µm) closely following large droplets ($d_p > 20$ µm) was determined by time and distance between them. A negligible velocity–distance correlation proved no wake effect on the small tracers.

Particles in the size bin 20–40 µm with Stk ~ 1 are still somewhat affected by the airflow while the largest particles (80–160 µm) with Stk > 10 should move almost ballistically.

The overall analysis shows that Stk decreases systematically with axial distance (Figure 6) for all size

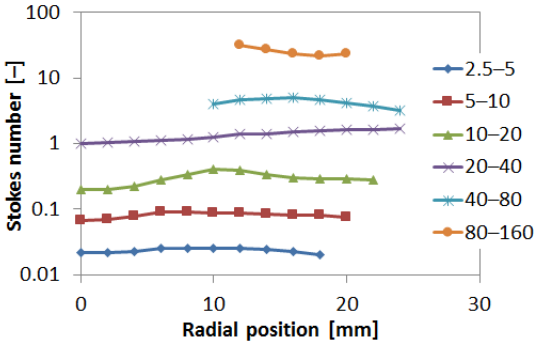

Figure 5. Droplet Stokes number in several size bins (indicated in µm); X = 25 mm, Δp = 1 MPa.

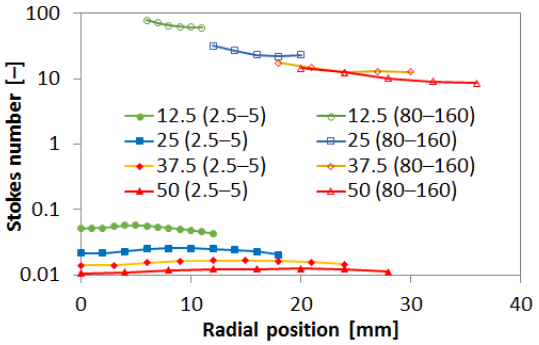

Figure 6. Stk of droplets in size bins 2.5–5 µm and 80–160 µm; at the four axial positions (in mm), Δp = 1 MPa.

groups (only 2.5–5 µm and 80–160 µm are displayed); the Stk reduces by ~ 7 with the axial position change from 12.5 to 50 mm. All the Stk features found for Δp = 1 MPa are also valid for 0.5 and 1.5 MPa; the Stk magnitude just increases moderately and systematically with Δp so that the corresponding Stk values for Δp = 1.5 MPa are approximately 1.8 times those for 0.5 MPa.

Size-Resolved Droplet Velocity

As mentioned earlier, the smallest particles attain the airflow velocity relatively quickly, and the upper size limit of such decelerated particles increases with axial distance downstream. The momentum transfer gradually affects all size classes so even the largest particles lose their kinetic energy with axial distance, Figure 7 top.

The root-mean-square fluctuating (rms) velocity (Figure 7 bottom) at the axial position of 12.5 mm shows a negative correlation with size suggesting that at this position the air is already relatively turbulent due to mixing with the liquid. The rms velocity of the largest particles represents nearly the level of original fluctuations at the exit orifice, ~ 4.4 m/s, and these are by 30% lower than the air

[1] Taken from measurements in X, Y and Z directions.

[2] Where d_{pi} is the diameter of an i-th particle, for each size class $d_{p\min} \le d_p < d_{p\max}$ and $d_{p\max}/d_{p\min} = 2$. Only points with more than 80 particles are shown.

[3] Tracing accuracy errors are below 1% for Stk < 0.1 according to Tropea et al. (2007).

[4] For example (Santolaya et al., 2013) in a similar case generated aerosol with D_{10} = 3.4 µm.

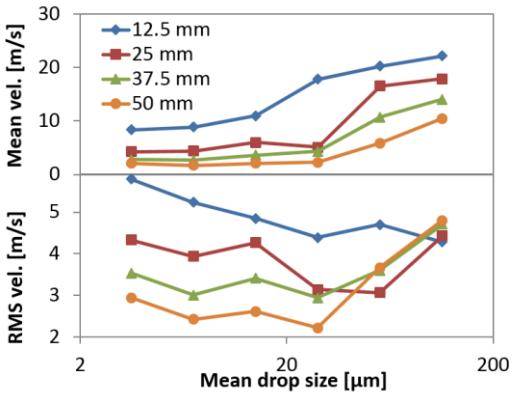

Figure 7. The size-resolved magnitude of the mean (top) and rms (bottom) velocity; r = 0.56, Δp = 1 MPa.

fluctuations. It illustrates that the gas–liquid mixing contributes to the turbulent flow more than the rms fluctuations introduced by the liquid itself. These fluctuations contribute to the droplet coalescence as well and also the preferential dispersion radially of the smaller particles

Liquid and Gas Velocity Fields

The mean velocity of the liquid mass in the spray was estimated as a volume-averaged particle velocity:

$$v_l = \sum_{i=1}^{n} d_{pi}^3 v_{pi} \Big/ \sum_{i=1}^{n} d_{pi}^3 \qquad (2)$$

in the axial, radial and tangential directions, with respect to the nozzle mean axis, and it represents the liquid momentum.

The velocity field of the liquid mass is compared with the gas velocity in Figure 8. The flow fields are similar in nature for all three operational pressures. The temporal mean, indicated below as "mean" only, for the axial and radial velocity components of both the phases are approximately ten times larger than the corresponding tangential (azimuthal) component. The swirling internal motion is almost fully converted into the radial liquid velocity component outside the nozzle and only the air-core (see Figure 1) swirl together with the residual rotational energy of the continuous liquid sheet, carried due to liquid viscosity forces, are transformed into a weak air swirl flow.

The radial distribution of the mean liquid velocity magnitude at X = 12.5 mm shows a single peak profile with the maximum in the direction of broken liquid sheet. The velocity decays, due to momentum transfer from the liquid phase into the originally quiescent air, with axial distance downstream from the nozzle and the profiles flatten. The droplets are decelerated by the air drag as $a = -(v_d - v_g)18\mu_g / \rho_l d_p^2$ establishing a positive size–velocity correlation. The smallest particles, 3 to 5 times slower (Figure 3 and 9) relative to the largest ones may lead to droplet collisions and coalescence in the dense spray region (Santolaya et al., 2013). A second velocity peak

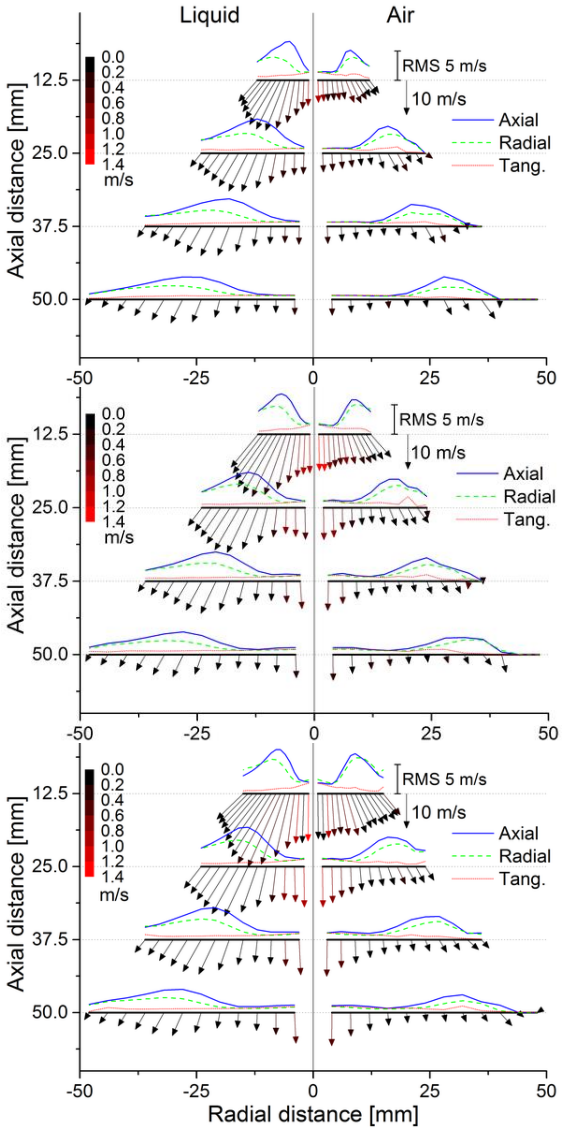

Figure 8. The velocity of liquid mass (left) and air (right), mean values in axial-radial directions shown as vectors colour coded according the tang. component, rms values shown as lines, Δp = 0.5, 1, 1.5 MPa (top to bottom).

appears at X = 37.5 mm and further downstream due to air support. The mean air velocity profiles show a near insignificant peak in the "sheet position" as well, but only for Δp = 0.5 MPa. The profiles at the higher pressures keep their maxima, which increases with Δp, along the spray centreline. The velocity magnitude decreases with radial distance due to momentum transfer and radial spreading of the spray cone.

The profiles of the rms axial and radial liquid velocity components generally behave in a similar manner and show

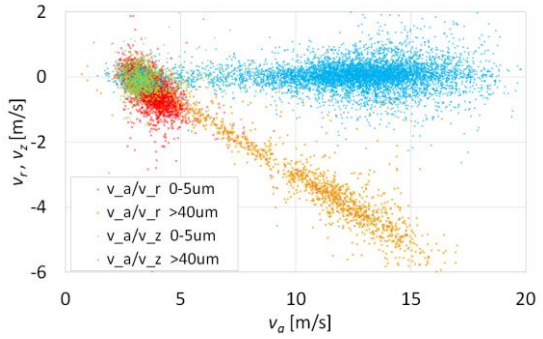

Figure 9. Velocity correlation, position X = 37.5 mm, R = 15 mm, Δp = 1 MPa.

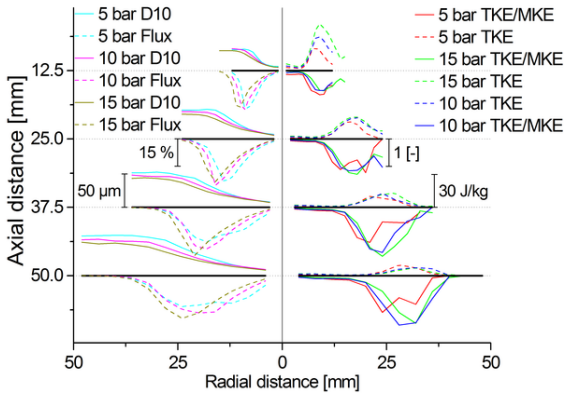

Figure 10. Liquid mass flux and D_{10} (left), TKE and TKE/MKE in the air (right).

a single peak maxima at relative radial distances of $R/X \approx 0.5$–0.6 depending on Δp. The maximum radial component is some 30–50% lower than the axial component. The tangential component is in most radial positions much lower than the other two, and its profile is rather flat or decreasing with increasing radius. The axial and radial profiles converge in the outer spray border ($r \approx 1$) while all three components coincide near the spray cone centreline.

The profiles of all three air rms components form a plateau which spreads from the spray centreline up to r = 0.4–0.5 (depending on Δp) with almost identical levels. These agree with centreline values of liquid rms velocity due to the simple fact that droplet size in the direction towards the centreline decreases to values for that Stk < 1 and such particles are controlled by the airflow. The rms velocity values are low in comparison with local mean velocity and also with the rms velocity outside this region. The axial and radial air rms components increase at positions r > 0.4–0.5 out to their maxima at $r \sim 0.6$ and then continuously decrease toward the spray outer border. The axial component is ~ 1.1–1.3× larger than the radial one. The rms components undergo a spreading and decay with axial distance downstream, but the decay is less significant in comparison with the mean component.

The flow field in the spray can be divided into three regions based on the airflow character: 1) an inner conical core at r < 0.4–0.5 where a compact flow with homogeneous turbulence of low level appears, 2) a semi-conical part of the main spray with high turbulence levels and strongly anisotropic fluctuations and 3) the low turbulence spray periphery. The air fluctuations are fed mainly in the second region (0.4–0.5 < r < 1) by the action of large, ballistic droplets, with Stk > 1. The mean velocity decays with axial distance downstream in regions 2 and 3 while, in the centreline area of region 1, the momentum is conserved downstream.

To understand better the character of the velocity fluctuations a correlation of the velocity components for a set of small ($d_p \leq 5$ µm) and large ($d_p \geq 40$ µm) droplets in an arbitrary mainstream position was generated in Figure 9. The axial-radial velocity correlation for large droplets is very strong. It indicates that the velocity fluctuations of the liquid mass, that induce the air fluctuations, appear mainly in the direction of the dominant spray movement. Similarly, it applies to the axial-tangential velocity correlation for large droplets. Small particles provide weaker correlation in both cases which suggests that the induced, strongly directional, fluctuations of the air tend to be more isotropic. This feature is in agreement with results in Figure 8 where smaller differences between the air rms velocity components are found in comparison with the liquid ones.

The rms component of axial air velocity is of the same magnitude as the mean value while the radial and tangential rms components are even larger than their mean counterparts. The magnitude of the air fluctuations indicates that this highly turbulent flow will significantly affect the small droplets in the axial direction in the area near the spray axis and in the radial direction in the off-axis radial areas.

Mean and Turbulent Kinetic Energies

The turbulent and mean kinetic energies, TKE and MKE respectively, are estimated using the velocity data of droplets with d_p < 5 µm. The radial TKE and TKE/MKE distributions (Figure 10) confirm that the TKE is concentrated in the second, main stream, spray region. Its maximum position corresponds to the area of maximum liquid flux. The TKE is only influenced by Δp only at X = 12.5 mm; for larger X values the TKE levels are similar. Such a low dependence on X can be explained by two counteracting pressure-related factors to the air flow: the size and velocity of the droplets.

Power Spectra Density of Velocity Fluctuations

The air–particle interaction and particle dispersion depends also on spectral properties of the flow fluctuations. The particle velocity data were used for estimation of the power spectral density (PSD) of the velocity fluctuations. The irregularity of the sampling time in PDA measurements,

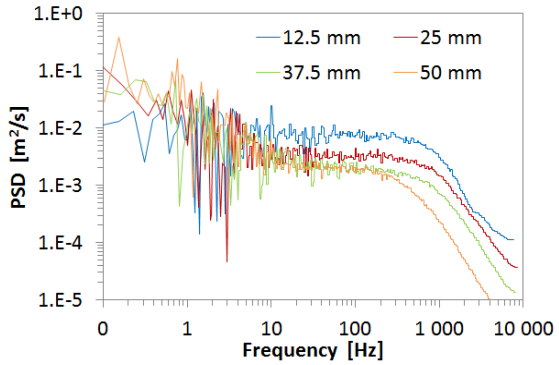

Figure 11. PSD of axial velocity fluctuations, all drop-size classes; r = 0.4 mm, Δp = 1 MPa.

a natural of the spray, does not allow direct application of an FFT for the PSD estimation. The slot correlation technique (Benedict et al. 2000) was tested to calculate the PSD. This approach produced limited results an interpolation with equidistant resampling, and common FFT was applied here. An averaging of the plot spectra was provided over the frequency bandwidths of Δf as: $\Delta f(f) = \pm 0.02f$.

The amplitude frequency characteristics of the PSD for the velocity fluctuations was processed for all Δp values, axial positions and all three velocity components at r = 0.4. Their character contains some features generally similar for all the data set (see Figure 11); the fluctuation level is high in the low-frequency band (f = 0.1–10 Hz), while for the following bandwidth, up to ~ 300–1,000 Hz, is flat and the last part features a monotonic decrease with frequency. The PSD level in the first bandwidth does not vary with axial distance, while for the other two bandwidths the levels systematically decrease downstream from the nozzle.

The fluctuation spectra of the tangential velocity component (not shown due to space limitations) is similar to the other two components up to $f \approx 10$ Hz but decreases more steeply with frequency in the upper spectral range. The effect of Δp on PSD is insignificant. Fluctuation levels of all drop-size classes are similar up to $f \approx 10$ Hz, but large particles, in most cases show significantly larger axial and radial velocity fluctuations for $f > 10$ Hz than the small particles. An insignificant, or even opposite size effect was found for the tangential velocity fluctuations.

SUMMARY AND CONCLUSIONS

The liquid and air flow fields in spray produced by small PS atomizer were investigated on an atmospheric spray bench using PDA. A Stokes number analysis of the sprayed droplets showed that particles sized below 5 µm follow the airflow faithfully so their velocity were used to provide an estimate of the local air velocity. The Stk increases with drop size, particles sized 20 to 40 µm (Stk ~ 1) are still somewhat influenced by the airflow while the largest ones, (80–160 µm, Stk > 10) moved move ballistically. The Stk varies insignificantly with the radial position but reduces ~ 10× for all size groups when the axial position increases from 12.5 to 50 mm. The Stk systematically increases with Δp so that values for Δp = 1.5 MPa are approximately 1.8 times greater than those for 0.5 MPa.

The liquid and gas velocity flow fields were compared in terms of their mean and rms velocities. The droplets are decelerated by the air drag establishing positive size–velocity correlation. The small particles, 3–5× slower than the largest ones, may lead to droplet collisions and coalescence in the dense spray region. Three distinct regions were identified based on the airflow character: 1) an inner conical core with a compact flow and low homogeneous turbulence, 2) a semi-conical part of the main spray with high turbulence levels and strongly anisotropic fluctuations and 3) the outer, low turbulence, spray periphery.

ACKNOWLEDGEMENTS

The authors acknowledge the financial support from the project No. GA15-09040S funded by the Czech Science Foundation and the project LO1202 NETME CENTRE PLUS with the financial support from the Ministry of Education, Youth and Sports of the Czech Republic under the "National Sustainability Programme I".

REFERENCES

Benedict, L. H., Nobach, H., and Tropea, C. (2000). Estimation of turbulent velocity spectra from laser Doppler data. Meas. Science & Technology, 11(8), 1089-1104.

Domann, R., and Hardalupas, Y. (2002). Planar Droplet Sizing for Quantification of Spray Unsteadiness. Proc. of 18th ILASS-Europe.

Durdina, L., Jedelsky, J., and Jicha, M. (2014). Investigation and comparison of spray characteristics of pressure-swirl atomizers for a small-sized aircraft turbine engine. Int. J. of Heat and Mass Transfer, 78(0), 892-900.

Lefebvre, A. H. (1989). Atomization and sprays. New York: Hemisphere Pub. Corp.

Lefebvre, A. H., and Ballal, D. R. (2010). Gas turbine combustion alternative fuels and emissions. from http://www.crcnetbase.com/isbn/978-1-4200-8604-1.

Luong, J. T. K., and Sojka, P. E. (1999). Unsteadiness in effervescent sprays. Atomization and Sprays, 9(1), 87-109.

Jedelsky. J., Maly, M., Holub, M., and Jicha, M. (2015, In print). Some aspects of desintegration of annular liquid sheet in pressure-swirl Sprays. Proc. of CMFF'15.

Santolaya, J. L., García, J. A., Calvo, E., and Cerecedo, L. M. (2013). Effects of droplet collision phenomena on the development of pressure swirl sprays. International Journal of Multiphase Flow, 56(0), 160-171.

Tropea, C., Yarin, A. L., and Foss, J. F. (2007). Springer handbook of experimental fluid mechanics. Berlin: Springer.

Walzel, P. (1993). Liquid atomization. International Chemical Engineering; (United States); Vol. 33:1, pp: 46-60.